Earthquakes and Structures, *Vol. 12, No. 1 (2017) 109-118*
DOI: https://doi.org/10.12989/eas.2017.12.1.109

Probabilistic seismic performance assessment of self-centering prestressed concrete frames with web friction devices

Long L. Song[1,2a] and Tong Guo[*1]

[1]*Key Laboratory of Concrete and Prestressed Concrete Structures of the Ministry of Education, Southeast University, Nanjing, 210096, P.R. China*
[2]*College of Civil and Transportation Engineering, Hohai University, Nanjing, Jiangsu 210098, P.R. China*

(Received June 15, 2016, Revised September 20, 2016, Accepted December 2, 2016)

Abstract. A novel post-tensioned self-centering (SC) concrete beam-column connection with web friction devices has been proposed for concrete moment-resisting frames. This paper presents a probabilistic performance evaluation procedure to evaluate the performance of the self-centering concrete frame with the proposed post-tensioned beam-column connections. Two performance limit states, i.e., immediate occupancy (IO) and repairable (RE) limit states, are defined based on peak and residual story drift ratios. Statistical analyses of seismic demands revealed that the dispersion of residual drifts is larger than that of peak drifts. Due to self-centering feature of post-tensioning connections, the SC frame was found to have high probabilities to be re-centered under the design basis earthquake (DBE) and maximum considered earthquake (MCE) ground motions. Seismic risk analysis was performed to determine the annual (50-year) probability of exceedance for IO and RE performance limit states, and the results revealed that the design objectives of the SC frame would be met under the proposed performance-based design approach.

Keywords: self-centering; concrete frame; web friction device; probabilistic seismic performance; seismic fragility

1. Introduction

Conventional reinforced concrete moment resisting frames (RC-MRF) in highly seismic regions may sustain considerable residual deformations after earthquakes. These residual deformations are an important measure of post-earthquake functionality, and often used to determine the technical and economical reparability of building damage following an earthquake. Ramirez and Miranda (2012) found that the amplitude of permanent residual story drift contributes the most to the economic losses for ductile structures, and these ductile buildings have a greater probability of being demolished due to large residual deformations than experiencing a collapse when subjected to intense ground motions. For example, following the 1985 Mexico earthquake, many damaged RC-MRFs were demolished due to the technical and economic difficulties in retrofitting and repairing the buildings with large residual deformations (Rosenblueth and Meli 2012).

There have been several studies aiming at understanding the parameters influencing the residual deformations of single-degree-of freedom (SDOF) systems and simple frame structures. MacRae and Kawashima (1997) systematically studied the residual deformation demands of inelastic SDOF systems, and found that increasing the post-yield stiffness can greatly reduce residual deformations. Ruiz-Garcia and Miranda (2006) evaluated the residual displacement demands in moment-resisting frames and found that the residual drifts are strongly influenced by the frame deformation mechanism, system overstrength and the type of hysteretic behavior. In Christopoulos *et al.* (2003) and Pampanin *et al.* (2003), the residual deformations of SDOF and multi-degree-of-freedom (MDOF) systems with different hysteretic rules were investigated and a performance matrix, which combines both the maximum and residual deformations, was suggested. Ruiz-Garcia and Miranda (2010) proposed a probabilistic procedure to estimate residual drift demands in performance-based assessment of existing multi-story buildings, and residual drift demand hazard curves were derived. Design approaches to reduce residual displacements have also been proposed. Pettinga *et al.* (2007) showed that an elastic secondary system can be used to increase the post-yield stiffness of traditional framed and braced systems for the purpose of effectively reducing residual deformations. A dual structural system composed of flexible moment-resisting frames and buckling-restrained braces was proposed by Teran-Gilmore *et al.* (2015) to reduce residual drifts at the end of the main-shock excitation.

Recent research on self-centering (SC) seismic systems have shown that they sustain much less residual deformation and damage as compared with the conventional seismic force-resisting systems (Christopoulos *et al*. 2002, Ricles *et al*. 2001, Lin *et al*. 2013, Li *et al*. 2008, Solberg *et al*. 2008, Bradley *et al*. 2008, Rodgers *et al*. 2012, Morgen and Kurama 2007). Among these researches, self-centering concrete MRFs are being studied as a viable alternative to

∗Corresponding author, Professor
E-mail: guotong77@gmail.com
[a]Ph.D.
E-mail: sll523@126.com

http://www.techno-press.com/journals/eas&subpage=7 ISSN: 2092-7614 (Print), 2092-7622 (Online)

the traditional RC-MRFs in seismic regions. The research on self-centering concrete MRFs was initially conducted on the precast concrete structures under the PRESSS (PREcast Seismic Structural System) research program in the 1990s (Priestley 1991, 1996), where precast beam and column are assembled through unbonded post-tensioning tendons to provide the self-centering capabilities, while mild steel bars were grouted in ducts across beam-column joints (forming a "hybrid" connection) to provide the energy dissipation. The performance of precast concrete buildings with hybrid connections was verified through the cyclic testing of a 0.6-scale five-story precast concrete building (Priestley 1999). Subsequent researches on self-centering concrete MRFs devised other forms of energy dissipation elements, including tension-only mild steel devices (Li *et al*. 2008), external mounted mild steel devices (Solberg *et al*. 2008, Bradley *et al*. 2008), lead-based damping devices (Rodgers *et al*. 2012) and friction-based devices on the top and bottom surfaces of the beam ends (Morgen and Kurama 2007).

Recently, a novel self-centering beam-column connection, i.e., the self-centering prestressed concrete (SCPC) beam-column connection, has been proposed by Song *et al.* (2014). In this novel connection, unbounded post-tensioned (PT) strands are used to provide the self-centering (SC) capability and bolted web friction devices (WFDs) are installed at the beam ends to dissipate energy in earthquakes. The friction devices are located at the beam webs and thus have no interference with the floor slab, as compared with the connections developed by Morgen and Kuruma (2008). Moreover, steel jackets are shop fabricated at the beam ends, protecting the concrete from damage when the beam rotates relatively against the column.

Previous studies on self-centering concrete MRFs focused mainly on the development of beam-column connection, numerical modeling and structural response assessment in a deterministic way (Morgen and Kurama 2007). However, research on the potential benefits of residual deformation mitigation, particularly considering the uncertainties associated with the seismic events and structural responses, are insufficient. In this study, a probabilistic seismic performance evaluation procedure is used to assess the seismic performance of self-centering concrete MRFs with SCPC beam-column connections. To assess the probabilistic seismic response of self-centering frame structures, a case-study building structure is designed and analyzed by performing the seismic fragility and limit state probability analyses.

2. Structural model

2.1 Configuration and mechanical behavior

Fig. 1(a) shows a schematic representation of a MRF subassembly with SCPC beam-column connections. The SC-MRF has post-tensioned tendons running horizontally to the beam, which are anchored outside the exterior columns. Due to the initial post-tensioning forces applied to the tendons, the precast concrete beams are compressed against the concrete column to resist moments. Shear forces at beam ends are taken by friction forces at beam-column interfaces generated by PT tendons and at the web friction devices (WFDs). To protect the concrete at the beam-column interface from damage during rocking, the ends of the precast beam are armored with steel jackets and steel plates are embedded in the concrete column. Web friction devices are installed at the mid-depth of the beam to increase the energy dissipation capacity of the frame system. As shown in Fig. 1(d), the web fiction device consists of a steel channel and a steel connection plate, and is bolted through the connection plate to the column using the high strength bolts. As shown in Figs. 1(b)-(c), two shim plates were welded on the steel plate embedded in the column to ensure good contact between the beam and column (Song *et al.* 2014). Sandwiched between the outer channels and the steel jacket are two friction plates (i.e., brass or aluminum plates), which are attached to the inner surfaces of the steel channels. High strength friction bolts with washers compress the friction device and the steel jacket together and produce controlled normal forces on the friction surfaces. The diameter of the oversized circular bolt ducts in the steel jacket and concrete beam is much larger than that of the friction bolts to accommodate the relative motion of friction bolts when the beam rotates relative to the column.

The flexural behavior of a SC concrete beam-column connection with WFDs is characterized by the gap opening and closing at the beam-column interface under earthquake loading. Fig. 2(a) shows the free body diagram of a typical connection subassembly subjected to positive moment, where P is the resultant force of all tendons forces; F_f is the friction force resultant on the web friction device; N_c and V_c are the axial compressive force and shear friction force on the beam-column bearing interface, respectively; d_2 is the distance from the beam section centroid to the center of rotation (COR); and r is the distance between F_f and the COR; The connection moment M (at the beam-column interface) is contributed by two parts, M_{PT} and M_{Ff}, representing the contributions of PT tendons and web friction device, respectively, as follows

$$M = M_{PT} + M_{Ff} = P \cdot d_2 + F_f \cdot r \qquad (1)$$

A conceptual connection moment-relative rotation (M-θ_r) behavior of the SCPC connection under cyclic loading is shown in Fig. 2(b), where M = moment and θ_r = relative rotation upon gap opening at the interface between the beam and column. The beam-column interface is in complete contact until the applied external moment exceeds the imminent gap-opening moment M_{IGO} (at event 1 in Fig. 2(b)), which is equal to the sum of the moment resistance provided by the initial PT force and WFDs. As the load increases, gap-opening occurs and the connection rotational stiffness after gap opening is mainly provided by the PT tendons and can be determined by the depth of the beam, the axial stiffness and arrangement of the PT tendons, and the axial stiffness of the beam (Song *et al.* 2014). As θ_r increases, the PT tendons elongate to produce additional PT force, increasing the moment carried by the SCPC connection. PT tendon yielding occurs at event 3, as shown

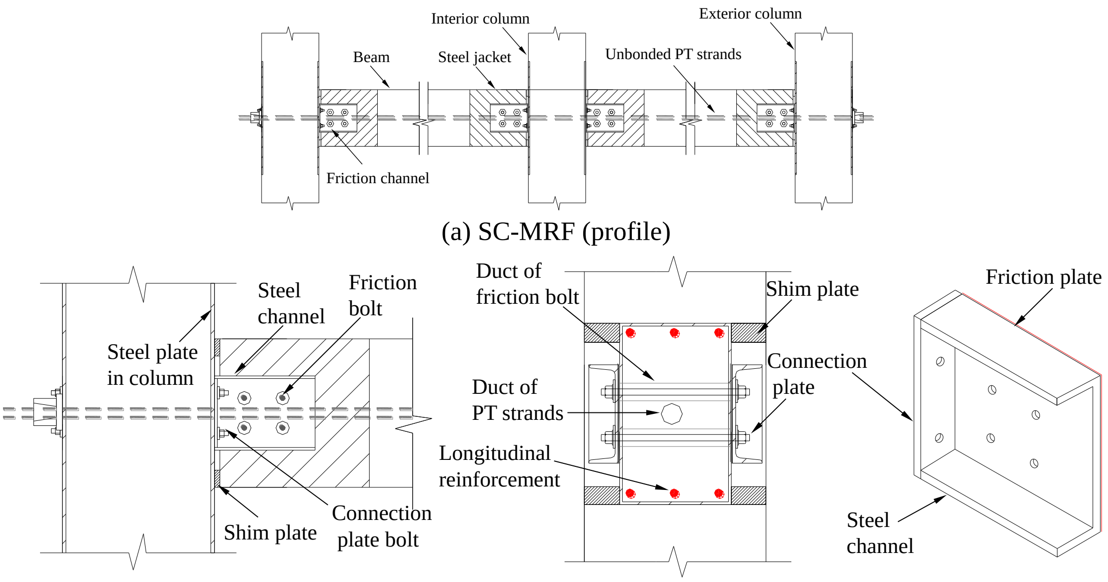

(a) SC-MRF (profile)

(b) SCPC connection (c) beam section (d) configuration of WFD

Fig. 1 Schematic illustration of a SC-MRF subassembly

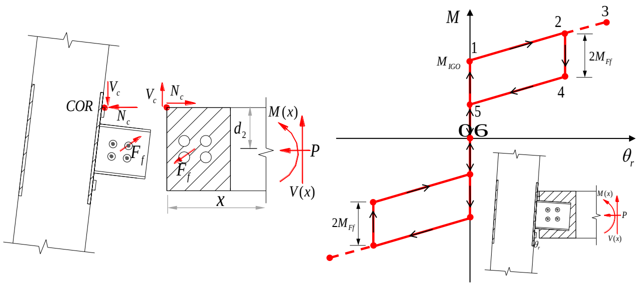

(a) Free-body diagram (b) Conceptual M-θ_r behavior

Fig. 2 SCPC beam-column connection with WFDs

in Fig. 2(b). If unloading at event 2 occurs, θ_r remains constant, where between events 2 and 4 the moment contribution of the connection changes direction due to a reversal of the friction force in the WFDs. The difference in moment between the event 2 and 4 is equal to two times the friction moment, M_{Ff}. Between the events 4 and 5, θ_r gradually reduces to zero as the beam come back in contact with the column. The connection moment decreases between events 5 and 6, and the connection return to its original position at event 6. A complete reversal of the applied moment will lead to a similar connection behavior in the opposite direction of loading, as shown in Fig. 2(b).

The energy dissipation required for the SCPC connection can be quantified by the effective energy dissipation ratio, β_E, which is the ratio of the energy dissipation of the self-centering system to the energy dissipation of a bilinear elastic-plastic system with the same force capacity (Lin *et al*. 2013). Based on Fig. 2(b), β_E can be calculated for design purposes, as follows

$$\beta_E = M_{Ff} / M_{IGO} \tag{2}$$

It can be seen that a larger β_E means that more energy is dissipated by the WFDs, and ACI Innovation Task Group (2001) recommends that β_E should be no less than 0.125. On the other hand, to maintain self-centering ability of the SCPC connection, β_E should be no greater than 0.5. Previous study (Song and Guo 2014) has shown the increase of β_E would result in reduced deformation of SC-MRF.

2.2 Prototype building

A performance-based design procedure adapted from Guo and Song (2014) was used for the design of the SC frame studied in this paper. The design approach uses two performance levels: Immediate occupancy (IO) and Repairable (RE). The IO performance level is a damage state that does not require structural repair, and the RE performance level is a damage state where only limited structural damage may have occurred and structural repairs may be required prior to re-occupancy. The design procedure considers two levels of ground motion intensity: the maximum considered earthquake (MCE) ground motion, and the design basis earthquake (DBE) ground motion. The design objectives are to be structurally damage free under the DBE, creating the potential for IO performance level, and to permit member yielding under the MCE, achieving RE performance level. To be more specific, under the DBE, the SC connection gap opening and minimal yielding at the column bases are allowed. Under the MCE, significant member yielding and steel jackets local yielding are permitted. However, PT strand yielding is not expected.

Using the performance-based design approach described above, a 6-bay, 6-story prototype office building with four-bay perimeter SC-MRFs was designed. Figs. 3(a)-(b) show the plan and elevation views of the prototype building, respectively. The building layout is adopted from the layout of post-tensioned steel moment resisting frame systems suggested by Garlock (2002). The building utilizes two SC moment resisting frames with the proposed post-tensioned

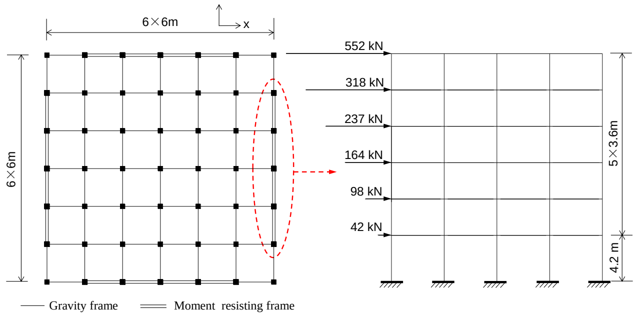

(a) Plan view (b) Elevation

Fig. 3 Plan view and elevation of the prototype building

Table 1 Design Characteristics of RC and SC frames

Floor	Beam size (mm×mm)	Column size (mm×mm)	T_0/kN	A_{SC}/mm^2	A_{sb}/kN	A_{PT}/mm^2	F_f/kN
6	400×600	550×550	366	2455	680	834	140
5	400×600	550×550	638	2946	680	834	245
4	400×600	550×550	870	3437	680	973	334
3	400×650	600×600	1005	3437	737	1112	398
2	400×650	600×600	1074	3928	737	1112	425
1	400×700	650×650	1068	3928	794	1251	434

beam-column connections as the seismic force resisting system in each of the two principal directions. Note that the slab was assumed to provide no restraint to gap opening at the PT connections, which can be achieved by the connection details proposed by Kim and Christopoulos (2009). The total building height is 22.2 m, with a first story height of 4.2 m and 3.6 m story heights for the upper stories. The type of soil at the building site was Class II, which corresponds to a rock or stiff soil site. The design dead loads are 4.5 kN/m^2 and 6.5 kN/m^2 for the floors and the roof, whereas the live loads for the floors and the roof are 2.0 kN/m^2, resulting in a total seismic weight of 45360 kN. The design base shear, V_{base}, was 1410 kN. The prototype frame was designed under a load condition of 100% of design dead loads plus 50% of design live loads to represent the gravity loads, combined with earthquake-induced lateral loads, as shown in Fig. 3(b). The design of the structural concrete members follows the National Standard of the People's Republic of China, Code for Design of Concrete Structures (GB 50010-2002 2002).

The design unconfined concrete strength is f_c=41.4 MPa, yield strength of PT strands is f_{py}=1675 MPa, and ultimate strength of PT strands is f_{pu}=1,862 MPa. The design moment demand at beam ends, M_d (corresponding to the imminent gap opening moment, M_{IGO}), can be determined from a linear elastic analysis of the structure under load combinations that included gravity loads and equivalent lateral forces corresponding to design base shear, V_{base} (Guo and Song 2014). Table 1 summarizes the design parameters of the prototype SC frame, where T_0 denotes the total initial PT force, A_{SC} denotes the column reinforcement ratio, A_{PT} denotes the area of PT tendons and F_f denotes the friction forces on the web friction devices. According to Eq. (1), the connection design moment, M_d, is satisfied by M_{PT} and M_{Ff}, representing the moment resistance of PT forces and friction forces, respectively. The PT tendons are placed at the beam centroid. β_E=0.20 is used in Eq. (2) and, with the combination of Eq. (1), to determine the value of T_0 and F_f. The area of PT tendons (A_{PT}) can be determined considering that PT tendon yielding should be prevented under the MCE. The beam reinforcement ratios (A_{sb}) are determined according to constructional reinforcement ratio.

2.3 Analytical models

Nonlinear time-history analyses were performed on the 6-story SC frame using the finite element structural analysis program OpenSees (Open System for Earthquake Engineering Simulation) (Mazzoni *et al* 2009). A two-dimensional plane frame consisting of only one MRF was modeled and analyzed in this study. Fig. 4 shows a schematic representation of the SC frame model, which is developed based on the SCPC beam-column connection model described in Song *et al.* (2014). The beam column interface was modeled using two pairs of rigid elements, which were based on the elasticbeamcolumn element in OpenSees assigned with large axial and bending stiffness. The gap opening and closing mechanism at the beam-column interface was modeled using a pair of zeroLength contact elements with compression only material properties. The node of beam element at the beam-column interface was slaved to the panel zone side node in the vertical direction to transfer shear force. The beam-column panel zone was modeled using a group of rigid elasticbeamcolumn elements located at four sides of the panel zone and a rotational spring positioned at one of the four corners. The steel channel was modeled using an elasticBeamColumn element in OpenSees so that the flexibility of the channel could be simulated. The friction force was modeled using a zeroLengthSection element incorporated with bi-directional plasticity properties. Post-tensioned tendons were modeled using truss elements running parallel to the beam axis and a bilinear material model with an initial strain was applied to the truss elements. To simulate the rupture of tendons, an ultimate strain was assigned to the bilinear material model of PT truss element.

The beams and columns of the SC frame were modeled using the distributed plasticity fiber elements which can capture the distribution of inelasticity across the depth of the section and the length of the physical member. Each section of the members

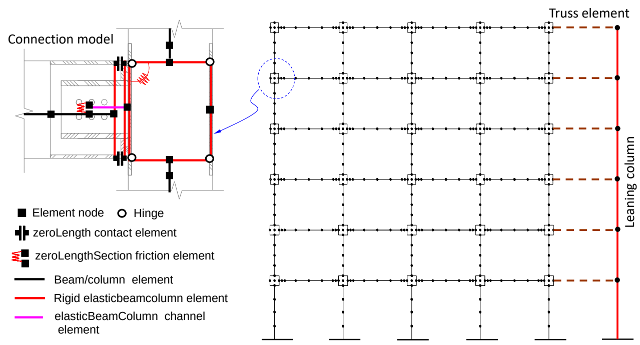

Fig. 4 Analytical model of the SC frame

is subdivided into a number of fibers assigned with the uniaxial stress-strain relationships of the materials. The Giuffre-Menegotto-Pinto hysteretic material in OpenSees is used to model the reinforcing steel. The transverse confinement effect to the core concrete of members is accounted for by increasing strength and deformation capacity of concrete using the Kent-Scott-Park model (Kent and Park 1971).

The P-delta effects from the building interior gravity frames were incorporated in to the SC frame model through a lean-on column, as shown in Fig. 4. The vertical axial forces due to gravity loads were applied to the beam spans and the lean-on columns of both frames. Rayleigh damping was applied with a damping ratio of 5% specified at the first and third structural modes. In order to adequately capture the residual deformation, all analyses are performed with additional zero acceleration values padded total ground motion records to allow the free vibration decay of the structure.

3. Framework for probabilistic seismic performance assessment

3.1 Equations for performance assessment

The probabilistic seismic performance assessment identifies the responses of a structure with a consideration on the uncertainties associated with the seismic events and the subsequent structural responses. It usually provides the probability that a structure exceeds a certain limit state (LS), which is used to identify the structural performance level. The limit state probability can be defined as

$$P_{\mathrm{LS}} = \sum_{x} P\left[\mathrm{LS}\middle|\mathrm{SI}{=}x\right] H\left(x\right) \tag{3}$$

where SI is the intensity of the seismic demand, measured in terms of ground motion (i.e., peak ground acceleration) or spectral (i.e., spectral acceleration) intensities; $P\left[\mathrm{LS}\middle|\mathrm{SI}{=}x\right]$ is the structural fragility, which describes the probability of reaching a structural limit state LS, given the occurrence of SI=x; and $H(x)$ denotes the seismic hazard, which is often represented by the mean annual frequency of the SI exceeding the value x and can be expressed as

$$H\left(x\right) = \mathrm{P}\left[SI > x\right] = k_0 x^{-k} \tag{4}$$

where k_0 and k are constants that are dependent on regions and site conditions of the building (Cornell *et al.* 2002).

Assuming that structural fragility can be modeled by a lognormal cumulative distribution function (CDF), which has been supported by many previous researches (Singhal and Kiremidjian 1996, Song and Ellingwood 1999), the fragility corresponding to a given damage state can be expressed as

$$F_{\mathrm{R}}(x){=}\Phi[\frac{\ln x - \ln m_R}{\beta_{\mathrm{R}}}] \tag{5}$$

where $\Phi[\cdot]$ is the standard normal probability integral; m_R denotes the median value of the structural fragility, expressed in terms of the control variable that are used to define the seismic hazard; and β_R denotes the logarithmic standard deviation of the system fragility. The dispersion parameter β_R reflecting uncertainties associated with seismic demand and structural capacity is calculated as following equation (Cornell *et al.* 2002)

$$\beta_R = \sqrt{\beta_{D|SI}^2 + \beta_c^2} \tag{6}$$

where the uncertainty in seismic demand, $\beta_{D\backslash SI}$, is represented by the dispersion in maximum or residual story drift ratios, and the uncertainty in structural capacity β_c is set equal to 0.3 (Wen *et al.* 2003).

Combining Eq. (4) and Eq. (5), Eq. (3) can be approximately rewritten as shown in following equation

$$P_{\mathrm{LS}} = (k_0 m_{\mathrm{R}}^{-k}) \exp[\frac{(k\beta_{\mathrm{R}})^2}{2}] \tag{7}$$

The P_{LS} calculated from Eq. (7) is the annual exceedance probability, while the following equation can be utilized to calculate the probability of exceedance in 50 years (Ang and Tang 2007)

$$P_{\mathrm{LS/50}} = 1 - (1 - P_{\mathrm{LS}})^{50} \tag{8}$$

3.2 Definition of limit states

The limit states selected for fragility analysis can be identified by different levels of an engineering demand parameter (EDP). Researchers have utilized displacement-based, energy-based and hybrid measures to quantify damage; however, there has been little consistency on the most appropriate measure (Park *et al.* 2009). ASCE/SEI 41-06 (2007) proposes the use of the maximum story drift ratio ($\theta_{\max}$) to evaluate building performance and damage levels of structural components. In this study, to evaluate the post-earthquake seismic performance of the SC-MRF, the residual story drift ratio (θ_{res}) is also used to fully quantify the performance level of the structures. According to Guo and Song (2014), two structural performance levels are adopted in this study, namely, Immediate occupancy (IO) and Repairable (RE) performance levels, with corresponding maximum allowable story drift ratios of 1.0% and 2.0%, respectively. The threshold residual story drifts for the “IO” and “RE” performance levels are 0.2% and 0.5%, respectively.

The maximum allowable drift ratios for the Immediate occupancy (IO) and Repairable (RE) performance levels are determined according to the Chinese code for seismic design of buildings (GB 50010-2002 2002). The residual drift limit of 0.2% for the “Immediate occupancy” performance level was adopted based on the acceptable out-of-plumb construction tolerance recommended by ATC (2009). The construction tolerance, typically found in the building codes, set limits for deviation from the designed column and beam lines to ensure that the performance of the structure is almost “as designed”. Previously, O’Reilly *et al.* (2012) used such a threshold value (i.e., 0.2%) as the re-centering criterion for the self-centering concentrically braced frame systems, indicating that the structure with such small residual drifts can be regarded the same as the one prior to the earthquake. The 0.5% residual drift limit for the “Repairable” performance level was determined based on a survey of damaged structures during past earthquakes (McCormick *et al.* 2008). It was found that when direct and indirect repair costs were considered along with losses due to building closure during the repair period, it was no longer practically suitable for repair from an economic perspective when residual drifts were greater than 0.5% rad.

3.3 Seismic hazard analysis

The probabilistic seismic hazard analysis (PSHA) yields the seismic hazard curve, which provides the annual exceedance probability of earthquakes with a specified seismic intensity level at a given site. The seismic intensity (SI) measure considered in this study was the spectral acceleration at the first mode period, $Sa(T_1)$. Wen *et al.* (2003) found that using $Sa(T_1)$ as a SI measure can reduce the dispersion in the seismic demand from a given earthquake ensemble, thereby reducing the number of ground motion records necessary to perform the probabilistic seismic demand analyses with adequate precision, as compared to the other SI measures such as peak ground acceleration (PGA) or velocity (PGV).

Fig. 5 shows the seismic hazard curve for the model structure, which is obtained by fitting a line to the three points defined by the $Sa(T_1)$ values and the corresponding annual frequencies of exceedence, namely, 1/50, 1/475, and 1/2475, respectively. The three annual frequencies of exceedence correspond to hazard levels of 63.2%, 10%, and 2% probability of exceedance (PE) in 50 years, respectively.

3.4 Earthquake ground motions

A series of nonlinear time history analyses (NTHAs) known as incremental dynamic analysis (IDA) (Vamvatsikos and Cornell 2002) were performed with a set of ground motion records for the performance evaluation. Twenty-six far-fault earthquake ground motions (see Table 2) are taken from the Pacific Earthquake Engineering Research Center database (2009) for nonlinear time-history analyses (NTHAs). The selection criteria of the ground motions were as follows: (1) magnitude of the earthquake Mw⩾6.5; (2) closest distance to the fault rupture

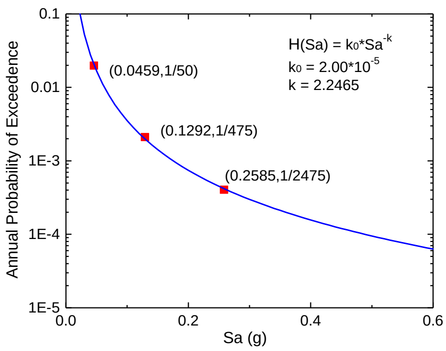

Fig. 5 Spectral acceleration hazard curve for the model structure

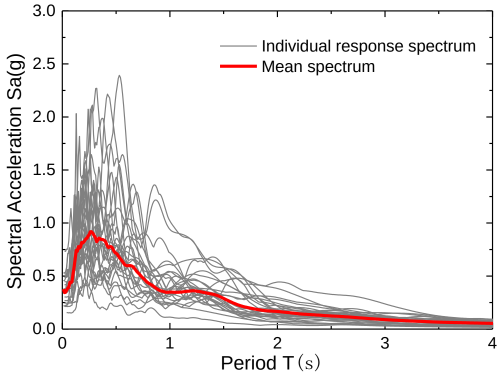

Fig. 6 Pseudo-acceleration spectra of selected ground motions

Table 2 Characteristics of selected earthquake records

No.	Year	Event	Component	Magnitude	Epicrntral Distance/km	PGA/g	Duration/s
1	1994	Northridge	MUL009	6.7	13.3	0.42	30
2	1994	Northridge	MUL279	6.7	13.3	0.52	30
3	1994	Northridge	LOS270	6.7	26.5	0.48	20
4	1999	Duzce, Turkey	BOL000	7.1	41.3	0.73	56
5	1999	Hector Mine	HEC000	7.1	26.5	0.27	45
6	1999	Hector Mine	HEC090	7.1	26.5	0.34	45
7	1979	Imperial Valley	H-DLT352	6.5	33.7	0.35	100
8	1979	Imperial Valley	H-E11140	6.5	29.4	0.36	39
9	1979	Imperial Valley	H-E11230	6.5	30.4	0.38	39
10	1995	Kobe, Japan	SHI000	6.9	46	0.24	41
11	1995	Kobe, Japan	SHI090	6.9	46	0.21	41
12	1999	Kocaeli, Turkey	DZC270	7.5	98.2	0.36	27
13	1999	Kocaeli, Turkey	ARC000	7.5	53.7	0.22	30
14	1992	Landers	YER270	7.3	86	0.24	44
15	1992	Landers	YER360	7.3	86	0.15	44
16	1989	Loma Prieta	CAP000	6.9	9.8	0.53	40
17	1989	Loma Prieta	CAP090	6.9	9.8	0.44	40
18	1989	Loma Prieta	G03090	6.9	31.4	0.37	40
19	1990	Manjil, Iran	ABBAR--T	7.4	40.4	0.50	46
20	1987	Superstition Hills	B-ICC000	6.5	35.8	0.36	40
21	1987	Superstition Hills	B-POE270	6.5	11.2	0.45	22
22	1987	Superstition Hills	B-POE360	6.5	11.2	0.30	22
23	1992	Cape Mendocino	RIO270	7.0	22.7	0.39	36
24	1992	Cape Mendocino	RIO360	7.0	22.7	0.55	36
25	1971	San Fernando	PEL090	6.6	39.5	0.21	28
26	1976	Friuli, Italy	A-TMZ000	6.5	20.2	0.35	36

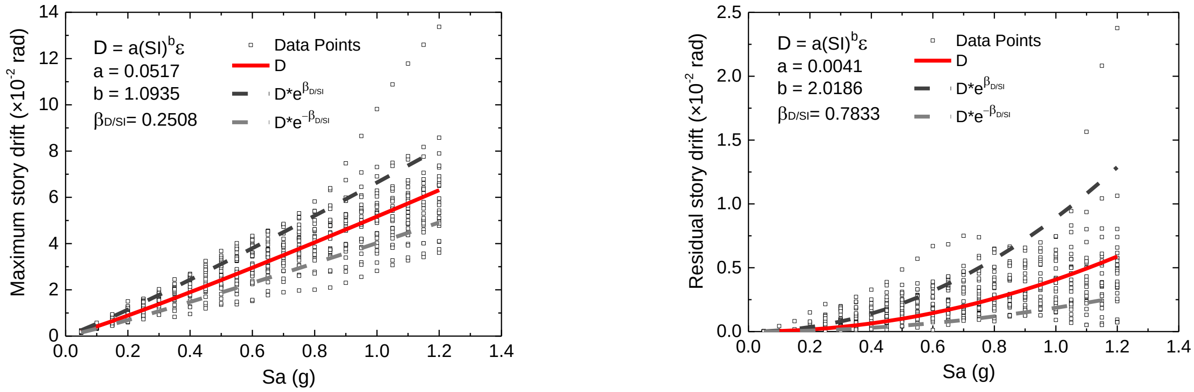

(a) Maximum story drift ratio (b) Residual story drift ratio

Fig. 7 Maximum and residual story drift demands vs. spectral acceleration relationship

10<Rrup<100 km; and (3) recording station site was classified as a rock or stiff soil site. These ground motions were found to have different peak ground accelerations (PGA), the first-mode spectral acceleration at 5% damping ratio, Sa(T_1,5%) and durations. Fig. 6 shows the spectra of the selected record set and the mean spectrum.

4. Seismic performance evaluation

4.1 Response statistics

The seismic demands (D) on the SC frames are determined from NTHAs performed using the input earthquake ground motions. For the probabilistic estimation of demand, the approach suggested by Cornell *et al.* (2002) is used, as follows

$$D = a\left(SI\right)^{b}\varepsilon \tag{9}$$

where a and b denote constants obtained from a linear regression analysis of seismic demand, ε is the lognormal random variable with a median of 1.0 and a logarithmic standard deviation of $\beta_{D/SI}$ which represents the dispersion of the demand.

The relationships between the structural demands (as measured by θ_{max} and θ_{res}) and spectral acceleration, Sa(T_1,5%), for the SC frame are presented in Fig. 7. The figure also shows the linear least squares regression results together with 16th percentile ($D{*}e^{\beta_{D/SI}}$) and 84th percentile ($D{*}e^{-\beta_{D/SI}}$) lines. Subjected to the MCE-level ground motions, the mean values of maximum and residual story drift ratios of the SC frame are 1.6% and 0.05%, respectively. According to the design objectives of the SC-MRF (Guo and Song 2014), which allows significant column base yielding and local yielding of steel jackets under the MCE, these residual drifts were mainly due to the yielding of the column bases and steel jackets. It should be noted that, when the SC frame was subjected to ground motions that exceed the MCE hazard level, PT strand yielding might occur, which will lead to the loss of self-centering capacity and subsequent residual rotations of post-tensioned connections.

The peak drift responses of SC frame exhibit a bit of softening with increasing seismic intensity, as apparent from the regression parameter b being slightly larger than 1. Note that the value of b equal to 1 means that the maximum drift ratio is linearly correlated with the seismic intensity measure, which is consistent with the *equal displacement rule* (Veletsos and Newmark 1960). The dispersions of maximum and residual drift demands are 25.08% and 78.33%, respectively, for the SC frame.

4.2 Seismic fragility and reliability

A fragility curve expresses the exceedance probability of a certain performance limit state as a function of a specific ground motion intensity parameter. The ground motion intensity is represented by the 5% damped spectral acceleration at the fundamental period of the structure and the performance limit states are measured in terms of maximum story drift ratio and residual story drift ratio. Previous studies have shown that, due to the material randomness on the variability in structural response is overshadowed by the randomness in the ground motions, the effect of material uncertainty on the seismic fragility is much less significant than the effect of ground motion characteristics (Kwon and Elnashai 2006, Jeong and Elnashai 2007). Therefore, the material randomness is ignored in the seismic fragility analysis in this study.

The seismic fragility curves of the SC frame for the IO and RE performance levels are presented in Fig. 8. Using the fragility curves, probabilities of exceedance (PE) corresponding to various limit states at 10% and 2% PE in 50-year earthquake hazard levels are calculated, as shown in Table 3. According to the Chinese code for seismic design of buildings (GB 50010-2002 2002), the DBE has a 10% probability of exceedance in 50 years, and the corresponding Sa at the fundamental period of the SC frame is 0.13 g. The MCE has a 2% probability of exceedance in 50 years, and the corresponding Sa is 0.26 g. It is observed from Fig. 8 that, when the maximum story drift ratio is used as the performance indicator, the probability of exceedance of the SC frame is 30.7% for the IO performance limit state, and decreases to 0.90% for the RE performance limit state for the earthquake level of 10% PE in 50 years. However, when the residual story drift ratio is used as the performance indicator, the

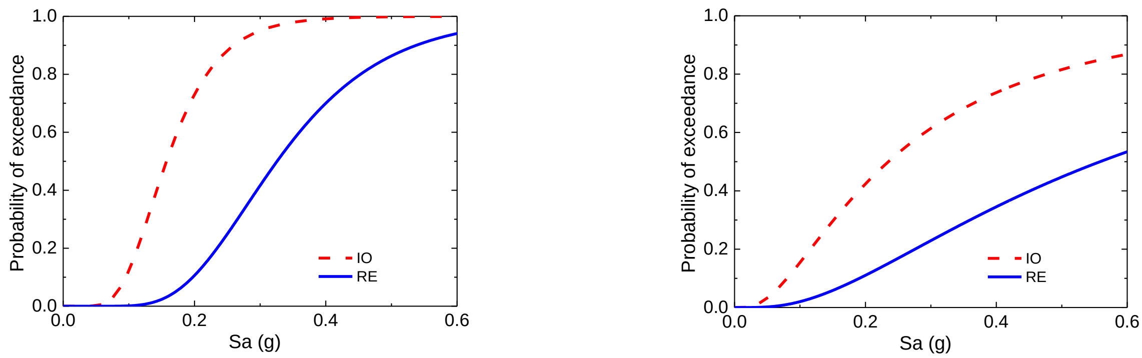

(a) Based on story drift (b) Based on residual drift

Fig. 8 Seismic fragility curves for the SC frame

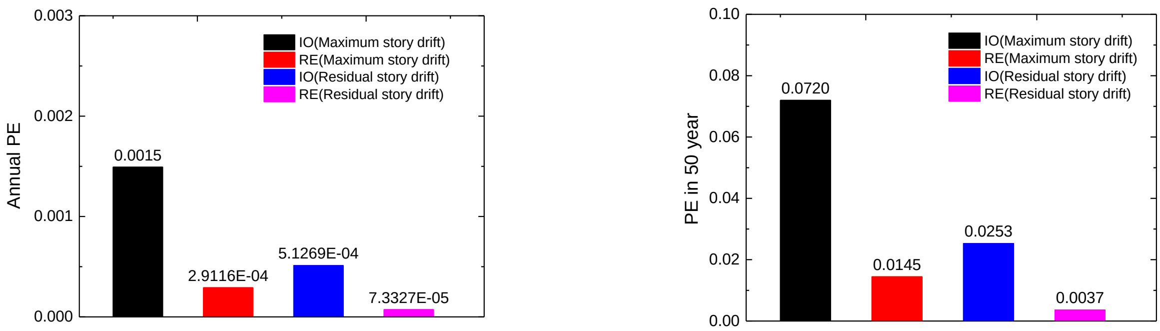

(a) The annual probability of exceedance (b) The 50-year probability of exceedance

Fig. 9 The annual and 50-year probabilities of exceedance (PE) for various limit states

Table 3 Probabilities of exceedance for various limit states

Earthquake level	Probability of exceedance (%, Peak drift)		Probability of exceedance (%, Residual drift)	
	IO	RE	IO	RE
DBE	30.705	0.901	6.180	0.506
MCE	89.786	27.703	23.792	4.049

SC frame has the probabilities of about 6.18% and 0.51% to realize the IO and RE performance levels, respectively, for the earthquake level of 10% PE in 50 years.

Seismic risk, which is usually measured annually or for a 50 year interval, is obtained by convolving the seismic fragility and seismic hazard curves. Fig. 9 shows the annual and 50-year probability of exceeding the various performance limit states for the SC frame.

According to the Chinese code for seismic design of buildings (GB 50010-2002 2002), the DBE and MCE level ground motions have 10% and 2% probability of exceedance (PE) in 50 years, respectively, with the structural uncertainty not considered. Therefore, the probabilistic seismic design objectives of the SC frame are to be the 50-year probability of exceedance of IO performance level being less than 10%, and the 50-year probability of exceedance of RE performance level being less than 2% (Yu 2012).

It is observed from Fig. 9 that, when the maximum story drift ratio is used as the performance indicator, the 50-year probabilities of exceedance are 7.20% and 1.45% for the IO and RE performance levels. When the residual story drift ratio is used as the performance indicator, the SC frame has the probabilities of about 2.53% and 0.37% for the IO and RE performance levels. It can be concluded that that the design objectives of the SC frame would be met under the proposed performance-based design approach.

5. Conclusions

Reinforced concrete frames designed according to current seismic design codes are expected to experience large residual deformation during large earthquakes, which reduces the post-earthquake functionality. In this paper, a self-centering (SC) concrete frame system, which uses a recently developed self-centering prestressed concrete (SCPC) beam-column connection, was proposed to mitigate residual deformations. To evaluate the proposed system, a prototype self-centering concrete frame is designed, modeled and assessed probabilistically. Incremental dynamic analysis has been performed to estimate the seismic demands (i.e., maximum and residual story drift ratios) using a set of selected earthquake records. Seismic fragility and reliability analyses are then conducted to assess the probabilistic seismic response of the prototype self-centering frame. Based on the presented analysis results, the following conclusions may be drawn:

• Subjected to the MCE-level ground motions, the residual story drift ratios of the SC frame were minimal. These residual drifts were mainly due to the yielding of the column bases and steel jackets.

• Statistical analyses of seismic demands reveal that the maximum drift ratio of the SC frame is approximately linearly correlated with the seismic intensity measure. However, the residual drift demand increases non-linearly with the increase of seismic intensity measure. In addition, the dispersion of residual drift demand is larger than that of maximum drift demand.

• To fully quantify the performance level of the self-centering frame structures, the maximum and residual story drift ratios are both used. Considering that there are no established seismic fragility evaluation criteria for the SC concrete frames, two limit states, i.e. immediate occupancy (IO) and repairable (RE) limit states, and the corresponding threshold values were defined in this study.

• Due to self-centering feature of post-tensioning connections, the SC frame was found to have high probabilities to be re-centered under the DBE and MCE ground motions. In addition, the SC frame showed lower probability of exceedence of the performance levels when the residual story drift ratio rather than the maximum story drift ratio was used as the performance indicator.

• Seismic risk analysis results revealed that the design objectives of the SC frame would be met under the proposed performance-based design approach.

Acknowledgements

The analytical work was supported by the National Key Research Program of China under Grant 2016YFC0701400, the Natural Science Foundation of China under Grants 51078075 and 51378107, Key Laboratory of Concrete and Prestressed Concrete Structures of the Ministry of Education at Southeast University, Scholarship Award for Excellent Doctoral Student of Ministry of Education of China and Excellent Doctoral Dissertation Foundation of Southeast University.

References

ACI Innovation Task Group (2001), "*Acceptance criteria for moment frames based on structural testing and commentary*", American Concrete Institute, Farmington Hills, Michigan.

Ang, A.H.S. and Tang, W.H. (2007), *Probability concepts in engineering: emphasis on applications to civil and environmental engineering*, (2nd Edition), John Wiley & Sons, Inc., New York, NY, USA.

Applied Technology Council (ATC) (2009), "Guidelines for seismic performance assessment of buildings: ATC-58 50% draft", Rep. No. 58, Applied Technology Council, Washington, DC, USA.

ASCE 41-06 (2007), "Seismic rehabilitation of existing buildings", American Society of Civil Engineers, Reston, Virginia.

Bradley, B.A., Dhakal, R.P., Mander, J.B. and Li, L. (2008), "Experimental multi-level seismic performance assessment of 3D RC frame designed for damage avoidance", *Earthq. Eng. Struct. Dyn.*, **37**(1), 1-20.

Christopoulos, C., Filiatrault, A., Uang, C.M. and Folz, B. (2002), "Posttensioned energy dissipating connections for moment-resisting steel frames", *J. Struct. Eng.*, **128**(9), 1111-1120.

Christopoulos, C., Pampanin, S. and Priestley, M.J.N. (2003), "Performance-based seismic response of frame structures including residual deformations. Part I: single-degree of freedom systems", *J. Earthq. Eng.*, **7**(1), 97-118.

Cornell, C., Jalayer, F., Hamburger, R. and Foutch, D. (2002), "Probabilistic basis for 2000 SAC Federal Emergency Management Agency steel moment frame guidelines", *J. Struct. Eng.*, **128**(4), 526-533.

Garlock, M. (2002), "Full-scale testing, seismic analysis, and design of post-tensioned seismic resistant connections for steel frames", Ph.D. dissertation, Civil and Environmental Engineering Dept., Lehigh Univ., Bethlehem, PA.

GB 50010-2002. (2002), "Code for design of concrete structures", Chinese code, Beijing, China. (in Chinese)

Guo, T. and Song, L.L. (2014), "Performance-based seismic design method of self-centering prestressed concrete frames with web friction devices", *J. Build. Struct.*, **35**(2), 22-28. (in Chinese)

Jeong, S.H. and Elnashai, A. (2007), "Probabilistic fragility analysis parameterized by fundamental response quantities", *Eng. Struct.*, **29**(6), 1238-1251.

Kent, D.C. and Park, R. (1971), "Flexural members with confined concrete", *J. Struct. Div.*, **97**(7), 1969-1990.

Kim, H.J. and Christopoulos, C. (2009), "Seismic design procedure and seismic response of post-tensioned self-centering steel frames", *Earthq. Eng. Struct. Dyn.*, **38**(3), 355-376.

Kwon, O.S. and Elnashai, A. (2006), "The effect of material and ground motion uncertainty on the seismic vulnerability of RC structure", *Eng. Struct.*, **28**(2), 289-303.

Li, L., Mander, J.B. and Dhakal, R.P. (2008), "Bi-directional cyclic loading experiment on a 3-D beam-column joint designed for damage avoidance", *J. Struct. Eng.*, **134**(11), 1733-1742.

Lin, Y.C., Sause, R. and Ricles, J.M. (2013), "Seismic performance of a large-scale steel self-centering moment resisting frame: MCE hybrid simulations and quasi-static pushover tests", *J. Struct. Eng.*, **139**(7), 1227-1236.

MacRae, G.A. and Kawashima, K. (1997), "Post-earthquake residual displacements of bilinear oscillators", *Earthq. Eng. Struct. Dyn.*, **26**(7), 701-716.

Mazzoni, S., McKenna, F., Scott, M.H. and Fenves, G.L. (2009), "OpenSees (Open system for earthquake engineering simulation)", Pacific Earthquake Engineering Research (PEER) Center, University of California, Berkeley.

McCormick, J., Aburano, H., Ikenaga, M. and Nakashima, M. (2008), "Permissible residual deformation levels for building structures considering both safety and human elements", *Proceedings of the 14th World Conference on Earthquake Engineering*, Beijing, China.

Morgen, B. and Kurama, Y.C. (2007), "Seismic design of friction-damped precast concrete frame structures", *J. Struct. Eng.*, **133**(11), 1501-1511.

O'Reilly, G.J., Goggins, J. and Mahin, S.A. (2012), "Behaviour and design of a self-centering concentrically braced steel frame system", *Proceedings of the 15th World Conference on Earthquake Engineering*, Lisbon, Portugal.

Pacific Earthquake Engineering Research Center (2014), "PEER Ground Motion Database", http://peer.berkeley.edu/peer_ground_motion_database.

Pampanin, S., Christopoulos, C. and Priestley, M.J.N. (2003), "Performance-based seismic response of frame structures including residual deformations. Part II: multi-degree of freedom systems", *J. Earthq. Eng.*, **7**(1), 119-147.

Park, J., Towashiraporn, P., Craig, J.I. and Goodno, B.J. (2009), "Seismic fragility analysis of low-rise unreinforced masonry

structures”, *Eng. Struct.*, **31**(1), 125-137.
Pettinga, D., Christopoulos, C., Pampanin, S. and Priestley, M.J.N. (2007), “Effectiveness of simple approaches in mitigating residual deformations in buildings”, *Earthq. Eng. Struct. Dyn.*, **36**(12), 1763-1783.
Priestley, M.J.N. (1991), “Overview of the PRESSS research program”, *PCI J.*, **36**(4), 50-57.
Priestley, M.J.N. (1996), “The PRESSS program-current status and proposed plans for phase III”, *PCI J.*, **41**(2), 22-40.
Priestley, M.J.N, Sritharan, S., Conley, J.R. and Pampanin, S. (1999), “Preliminary results and conclusions from the PRESSS five-story precast concrete test building”, *PCI J.*, **44**(6), 43-67.
Ramirez, C.M. and Miranda, E. (2012), “Significance of residual drift in building earthquake loss estimation”, *Earthq. Eng. Struct. Dyn.*, **41**(11), 1477-1493.
Ruiz-Garcia, J. and Miranda, E. (2006), “Evaluation of residual drift demands in regular multi-storey frames for performance-based seismic assessment”, *Earthq. Eng. Struct. Dyn.*, **35**(13), 1609-1629.
Ruiz-García, J. and Miranda, E. (2010), “Probabilistic estimation of residual drift demands for seismic assessment of multi-story framed buildings”, *Eng. Struct.*, **32**(1), 11-20
Ricles, J.M., Sause, R. and Garlock, M.M. (2001), “Posttensioned seismic-resistant connections for steel frames”, *J. Struct. Eng.*, **127**(2), 113-121.
Rodgers, G.W., Solberg, K.M., Mander, J.B., Chase, J.G., Bradley, B.A. and Dhakal, R.P. (2012), “High-force-to-volume seismic dissipators embedded in a jointed precast concrete frame”, *J. Struct. Eng.*, **138**(3), 375-386.
Rosenblueth, E. and Meli, R. (1986), “The 1985 Mexico earthquake: causes and effects in Mexico City”, *Concrete Int.*, (ACI), **8**(5), 23-34.
Singhal, A. and Kiremidjian, A.S. (1996), “Method for probabilistic evaluation of seismic structural damage”, *J. Struct. Eng.*, **122**(12), 1459-1467.
Solberg, K.M., Dhakal, R.P., Bradley, B.A., Mander, J.B. and Li, L. (2008), “Seismic performance of damage-protected beam-column joints”, *ACI Struct. J.*, **105**(2), 205-214.
Song, L.L. and Guo, T. (2014), “Study on seismic performance of self-centering prestressed concrete frames with web friction devices”, *China Civ. Eng. J.*, **31**(12), 47-56. (in Chinese)
Song, L.L., Guo, T. and Chen, C. (2014), “Experimental and numerical study of a self-centering prestressed concrete moment resisting frame connection with bolted web friction devices”, *Earthq. Eng. Struct. Dyn.*, **43**(4), 529-545.
Song, J. and Ellingwood, B.R. (1999), “Probabilistic modeling of steel moment frames with welded connections”, *Eng. J. (AISC)*, **36**(3), 129-137.
Teran-Gilmore, A., Ruiz-Garcia, J. and Bojorquez-Mora, E. (2015), “Flexible frames as self-centering mechanism for buildings having buckling-restrained braces”, *J. Earthq. Eng.*, **19**(6), 978-990.
Vamvatsikos, D. and Cornell, C.A. (2002), “Applied incremental dynamic analysis”, *Earthq. Eng. Struct. Dyn.*, **31**(3), 491-514.
Veletsos, A.S. and Newmark, N.M. (1960), “Effect of inelastic behavior on the response of simple systems to earthquake motions”, *Proceedings of the 2nd World Conference on Earthquake Engineering*, Japan.
Wen, Y.K., Ellingwood, B.R., Veneziano, D. and Bracci, J. (2003), “Uncertainty modeling in earthquake engineering”, FD-2 Rep. 12, Mid-America Earthquake (MAE) Center, Urbana, IL.
Yu, X.H. (2012), “Probabilistic seismic fragility and risk analysis of reinforced concrete frame structures”, Ph.D. Dissertation, Harbin Institute of Technology, Harbin. (in Chinese)

KT